Design and Evaluation of a 42-V Automotive Alternator With Integrated Switched-Mode Rectifier

Sai Chun Tang, *Member, IEEE*, David M. Otten, Thomas A. Keim, and David J. Perreault, *Senior Member, IEEE*

***Abstract*—This paper presents techniques for the design of high-power Lundell alternators with integrated switched-mode rectifiers. A multisection stator winding and interleaved rectifier arrangement is introduced that enables high power levels to be achieved using small semiconductor devices, and which greatly reduces the output filter capacitor requirements. We also demonstrate control methods suited for this interleaved system. In addition to accurate closed-loop output voltage control, we introduce methods to provide (partial) synchronous rectification for reduced loss, and to provide tight load-dump transient control. The proposed technology is validated in the design and experimental evaluation of a 42-V, 3.4-kW alternator with fully integrated power electronics and controls. The prototype alternator achieves approximately a factor of 2.1 increase in power and 1.6 increase in power density as compared to a conventional diode-rectified alternator.**

***Index Terms*—Integrated switched-mode rectifiers (SMRs), interleaved rectifier, 42-V automotive alternator, load-dump control.**

I. Introduction

THERE is an emerging need for automotive generators that can provide higher output power and power density, improved efficiency, and better transient response (including load-dump suppression.) Moreover, there is an interest in developing electrical systems at a higher voltage (42 V) to better accommodate more electrical power in automobiles, and to achieve economies available through tighter suppression of overvoltage transients. These challenges have motivated a variety of research into automotive alternator design in recent years (e.g., [1]–[26]).

Earlier work has shown that switched-mode rectification coupled with appropriate controls can provide dramatic improvements in the power capability, efficiency, and transient response of both Lundell and permanent magnet alternators [10]–[19], [24]–[26]. This paper, an extended version of [44], carries this strategy forward. We present the design and experimental evaluation of a high-power 42-V Lundell alternator having the power electronics and control circuitry fully integrated with the machine. The new design is shown to provide $\sim$100% increase in output power and power density over a conventional alternator design, along with significant improvements in load-dump transient performance. To achieve this, we introduce a multisection winding and interleaved rectifier arrangement that enables high power levels to be achieved using small semiconductor devices, and which greatly reduces the output filter capacitor requirements. We also demonstrate control methods suited to this interleaved system. In addition to accurate closed-loop output voltage control, we introduce means to provide (partial) synchronous rectification for reduced loss, and demonstrate the ability to achieve tight load-dump transient control within the requirements of 42-V electrical systems [27].

The paper is organized as follows: Section II reviews the general principles underlying the alternator design, and introduces the interleaved winding and switched-mode rectifier (SMR) structure we propose. The physical construction of the alternator system and integrated electronics is also described. Section III describes the control approach utilized with the interleaved architecture. Means for providing output voltage control are described, along with means for implementing synchronous rectification of the active devices. Experimental results demonstrating the efficacy of the control implementation are also presented. The load-dump protection control scheme implemented in the system is also described, along with experimental results demonstrating the ability to meet the requirements of 42-V systems. Finally, Section IV concludes the paper.

II. System Configuration

A. Switched-Mode Rectification and Load-Matching Control

Conventional three-phase Lundell alternators employ a diode bridge to rectify the generated ac voltages, and regulate the output voltage via field control. By exchanging the diodes in the bottom half of the rectifier bridge for active devices such as power MOSFETs, a semibridge SMR is obtained (see Fig. 1). The SMR provides additional means of controlling the alternator. As shown in [10] and elsewhere, by modulating the switches with an appropriate duty ratio (at a high frequency compared to the machine electrical frequency), the alternator output characteristics can be matched to the output in a manner that provides greatly increased power capability and efficiency across speed and power.

Manuscript received October 11, 2009; revised February 11, 2010; accepted March 27, 2010. Date of publication August 30, 2010; date of current version November 19, 2010. This work was supported in part by the member companies of the Massachusetts Institute of Technology/Industry Consortium on Advanced Automotive Electrical/Electronic Components and Systems. Paper no. TEC-00436-2009.

S. C. Tang is with the Focused Ultrasound Laboratory, Brigham and Women's Hospital, Harvard Medical School, Boston, MA 02466 USA (e-mail: sct@bwh.harvard.edu).

D. M. Otten, T. A. Keim, and D. J. Perreault are with the Laboratory for Electromagnetic and Electronic System, Massachusetts Institute of Technology, Cambridge, MA 02136 USA (e-mail: otten@mit.edu; tkeim@mit.edu; djperrea@mit.edu).

Color versions of one or more of the figures in this paper are available online at http://ieeexplore.ieee.org.

Digital Object Identifier 10.1109/TEC.2010.2050774

0885-8969/$26.00 © 2010 IEEE

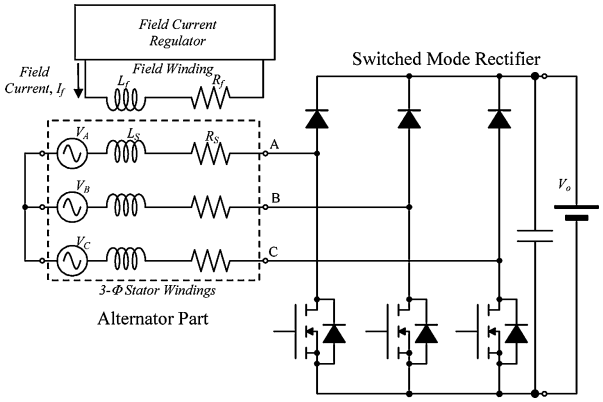

Fig. 1. Alternator with a semibridge SMR.

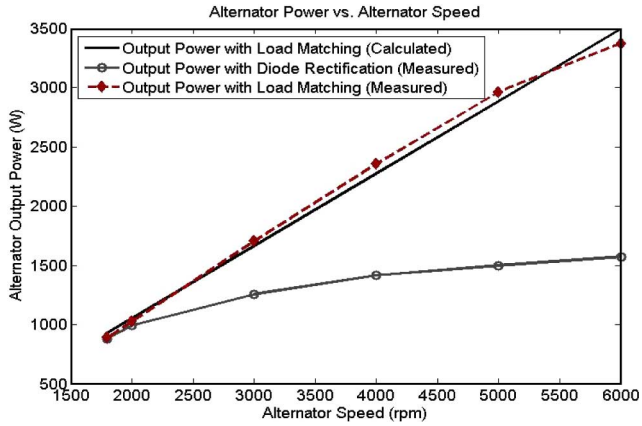

Fig. 2. Alternator power capability versus speed for diode rectification and for load matching control (e.g., with a SMR). Measured curves are for the alternator machine used in the prototype.

As shown in [10], the output power of an alternator with this SMR can be found as

$$P_{\text{out}} = \frac{3\,(1-d)\,V_o}{\pi}\,\frac{\sqrt{(k\omega i_f)^2 - \left(\frac{2(1-d)V_O}{\pi}\right)^2}}{\omega L_S} \qquad (1)$$

where

P_{out} alternator output power;
d duty ratio of the active switches;
L_s synchronous inductance of the stator winding;
ω alternator angular electrical frequency;
i_f alternator field current;
k machine constant (line-neutral back electromotive force (EMF) voltage magnitude $V_s = k\omega i_f$).

To obtain improved performance, duty ratio d is controlled up to a maximum value that provides load matching of the alternator [maximizing P_{out} in (1)]

$$d_{\text{match}} = 1 - \frac{\sqrt{2}\pi k}{4V_o}\omega i_f. \qquad (2)$$

By selecting appropriate combinations of duty ratio and field current, the alternator output power can be controlled up to a maximum that is a function of the alternator speed. The machine stator winding (which influences k and L_s) is selected to provide the desired capability for a specified output voltage V_o (e.g., 14 or 42 V)[1]. Fig. 2 shows the output power capability for the prototype Lundell machine (for an appropriate stator winding) with both diode rectification and load-matched operation (as with switched-mode rectification). As can be seen, the additional flexibility provided by the SMR yields tremendous improvements in output power capability across the speed range. Moreover, as shown in [10], this can be achieved at higher efficiency and *lower* operating temperatures.

B. Interleaved Alternator Design

While the use of switched-mode rectification offers major opportunities, it also poses some practical challenges. One issue to be addressed is the pulsating ripple current at the output of the SMR . Unlike a diode rectifier, the output current of the SMR of Fig. 1 pulsates at the switching frequency, yielding an rms ripple current into the rectifier output capacitor that is on the order of $I_o(d/(1-d))^{1/2}$, where I_o is the average alternator output current. Low equivalent-series-resistance capacitors with high ripple-current rating are, therefore, required to absorb this ripple current and contribute to electromagnetic interference (EMI) filtering. This is certainly achievable in a small volume using film or multilayer ceramic capacitors (see, e.g., [10]), but does represent a significant cost element. A second challenge relates to sizing of the semiconductor switches. At 14 V output, reasonably high-power alternators can be implemented with single-die plastic-packaged devices, owing to the wide availability of low-resistance 30- and 20-V MOSFETs for low-voltage applications. (we assume the use of active load-dump control techniques such as those demonstrated here or in [10] to enable use of low-voltage MOSFETs. Partly countering the advantage of MOSFETs at 14 V is the relatively worse performance of diodes at 14 V). At 42 V output, however, it is more difficult to realize the circuit of Fig. 1 without resorting to paralleled devices or devices modules (as used in [10]), especially when seeking to achieve high output power and temperature ratings.

Here, we demonstrate a design strategy that addresses both of the aforementioned challenges. Instead of the design of Fig. 1, we employ an interleaved machine and rectifier configuration, as illustrated in Fig. 3. In this approach, the system is constructed from a number N_C of small rectifier cells connected in parallel, with each cell fed from a separate isolated three-phase stator winding. The total system size and rating remains essentially unchanged, but utilizes more and smaller devices and windings. The switching patterns of the SMR cells are identical, but are each shifted in time from the other cells by T_{SW}/N_C, where T_{SW} is the SMR switching period. As will be shown, this provides significant advantages in filtering of the output. Interleaving has been applied earlier in a variety of applications, including dc–dc converters [28], [29], rectifiers [30], [31], and even in alternators [5] (albeit with different operating conditions and design objectives).

[1]Neglecting device drops and other second-order effects, the same power capability can be achieved at any specified output voltage V_o by an appropriate rewinding of the stator.

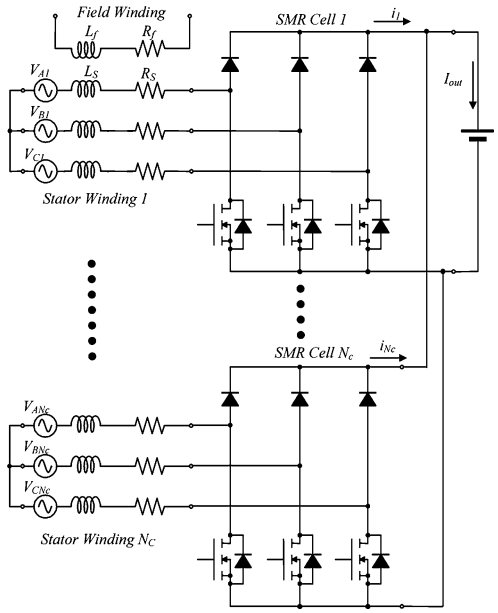

Fig. 3. Schematic of multiwinding machine and interleaved SMR.

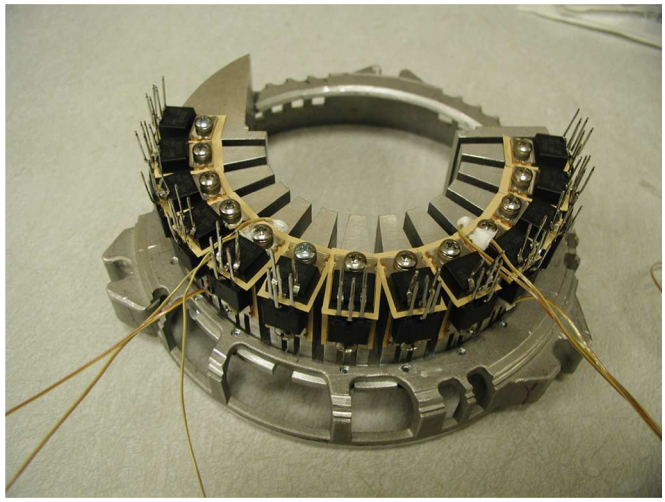

Fig. 4. Switching devices and heat sink for the prototype four-cell SMR system. The printed circuit board containing drive, control, and filtering circuitry mounts over this assembly.

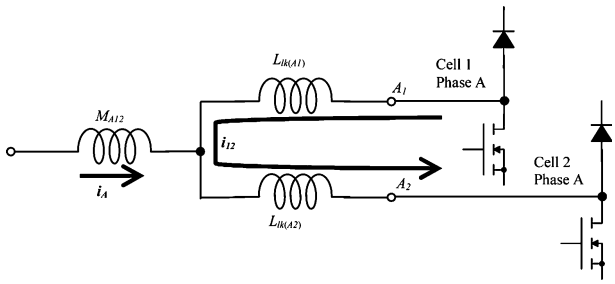

Fig. 5. Equivalent circuit model illustrating circulating currents among different rectifier cells due to magnetic coupling among the phase sets.

Interleaving has a number of advantages in the present design. First, high power can be achieved using multiple rectifier cells, each of which only require small, single-die devices in inexpensive packages. Moreover, the dissipation associated with rectification can be physically spread over a larger heat sink area, reducing the thermal management challenge. This can be seen qualitatively in the photograph of the distributed rectifier in our prototype system (see Fig. 4). A further major advantage of interleaving is the achievable reduction in output ripple and current rating of the output capacitor. Similar to the single SMR, each of the SMR cells delivers currents pulsating at the switching frequency. With interleaving, however, the *net* switching ripple current has a higher fundamental frequency (by a factor N_C) and its rms value is greatly reduced. This both greatly eases filtering of the output (e.g., to meet EMI specifications) and reduces the rms ripple rating of the alternator output capacitance. The degree to which ripple is attenuated depends on the number of cells employed and the duty ratio selected; the impact of this on control is considered in the following section.

C. Alternator Winding Design

The design described here is based on a modified Delco/Remy 92319 alternator (12-V, 130-A rating). The stator of the machine has 36 slots, into which the original three-phase winding was wave-wound. Each phase of the original machine comprised two parallel 14-AWG wires wound for a total of 72 series turns, yielding six turns (12 wires) per slot, with some slots containing an additional two wires for terminating the winding. The stator was rewound for the proposed interleaved SMR system at 42-V output. Rewinding of the machine focused on realizing the multiple three-phase sets for an interleaved system (see Fig. 3). A four-cell system was implemented having four separate sets of three-phase windings. Because our design incorporates a boost rectifier, the same number of turns (in each phase set) as the original 14-V alternator was used for 42-V output (see [10], [16], and [25] for the impact of turns count). The machine was rewound with each phase conductor comprising one strand of $17\frac{1}{2}$-AWG wire, yielding a copper packing factor close to that of the original machine.

In implementing an interleaved system, the magnetic coupling among different winding sets must be carefully considered in order to prevent undesirable circulating currents and losses [25]. In particular, it is desirable for the individual stator sets to be magnetically isolated to a large extent, to prevent differential ac circulating current among cells. Fig. 5 uses an equivalent circuit incorporating a transformer T model to illustrate the impact of magnetic coupling between the two phase-A windings for SMR cells 1 and 2. Since the MOSFETs are switching ON and OFF with a time shift, a differential ac voltage across terminals A_1 and A_2 results a circulating current i_{12} flowing through the winding leakage inductance, $L_{\mathrm{lk}(A1)}$ and $L_{\mathrm{lk}(A2)}$. This circulating current superimposes on the phase current i_A, and causes ripple currents at the SMR cells inputs. The magnitude of i_{12} is inversely proportional to the values of $L_{\mathrm{lk}(A1)}$ and $L_{\mathrm{lk}(A2)}$. Thus, in a case when the phase windings are wound in the same stator slots, the large mutual coupling and small leakage inductance lead to a large value of circulating current, and hence, ripple currents at the SMR cells inputs.

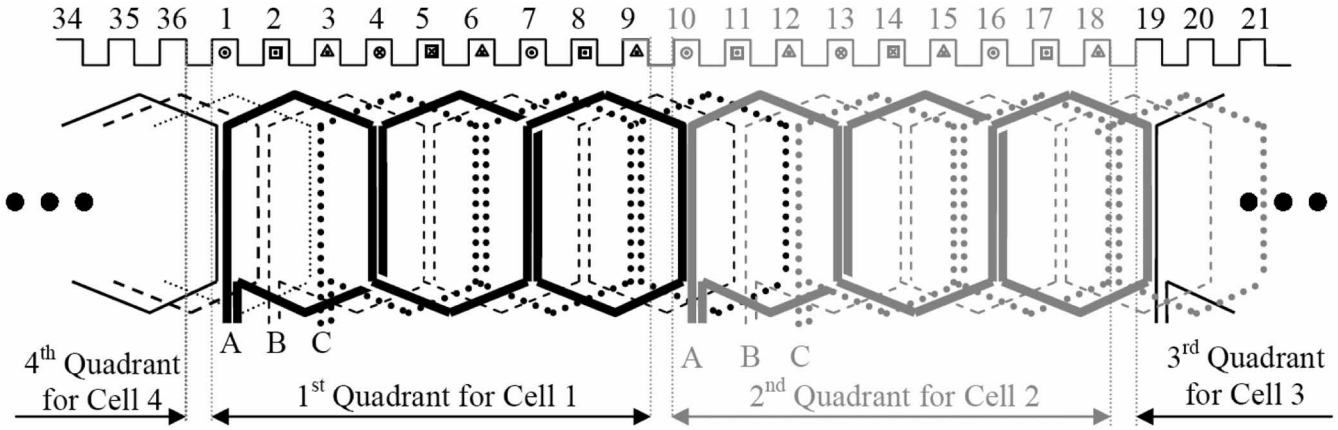

Fig. 6. Stator winding configuration for the four-SMR-cell alternator system. Each winding comprises 72 series turns made with $17\frac{1}{2}$-AWG wire (48 wires per slot). Adjacent sectors having different phase sets share only one slot, limiting magnetic coupling to a small value [25].

To address the issue of magnetic coupling, the four sets of windings were wound in four separate sectors of the machine, as illustrated in Fig. 6. Each phase winding occupies a quadrant of the stator spanning nine stator teeth. Because the number of slots for a phase winding is an odd number, windings of each phase in adjacent sectors share one stator slot. For example, as illustrated in Fig. 6, the two phase-A windings for SMR cells 1 and 2 share slot 10. As analyzed in detail in [25] and validated experimentally, this winding strategy limits magnetic coupling of different phase sets to a few percent, producing large leakage inductance and eliminating practical concerns about circulating current. The only disadvantage observed in this highly separated winding scheme is that any mechanical offset in the position of the rotor from the true center of the stator can yield differences in gap (and hence back EMF) among different phase sets. The back EMF variations that were encountered in practice were only on the order of 5%, however, which was found to be acceptable.

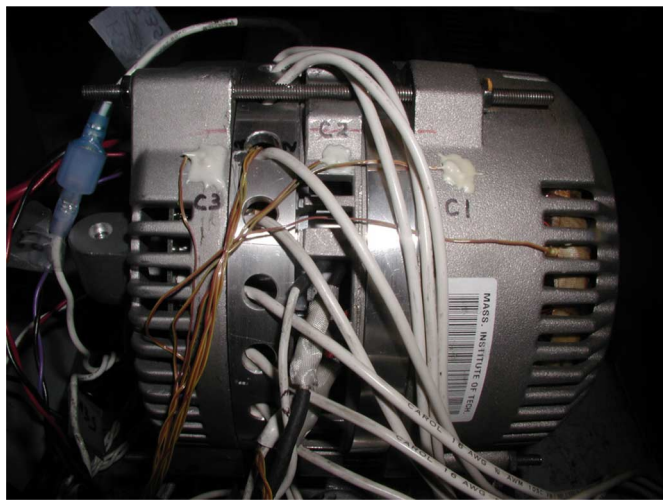

Fig. 7. The prototype four-cell alternator. The 42-V alternator and power electronics are completely integrated. Numerous voltages and temperatures are brought out for evaluation purposes.

D. Rectifier Design and Integration

The aforementioned rewound machine has been coupled with a four-cell ($N_C = 4$) SMR (see Fig. 3) to realize a 3.4-kW, 42-V alternator. This alternator has the power electronics and control circuitry fully integrated into the machine. To accommodate the prototype SMR, heat sink, and sensors, the alternator case was extended by approximately 4 cm (roughly by a factor of 1.3). As the redesigned alternator achieves a factor of 2.1 increase in output power (see Fig. 2), we have achieved more than a factor of 1.6 improvement in power density. (Based on our subsequent study, we believe that the rectifier could be incorporated with *no* increase in case length, promising over a factor of 2 improvement in power density.) A photograph of the prototype alternator (with thermocouples attached and internal node voltages brought out) is shown in Fig. 7.

Based on our design studies (including [17] and [23]–[26]), it is expected that a three-cell interleaved design would have been adequate for meeting the target performance and semiconductor thermal requirements to ambient temperatures beyond 85 °C. However, we developed the four-cell design to make better use of the available heat sink area and achieve higher temperature capability. Each of the four cells utilizes three IRFB4310 MOSFETs (100-V, 5.6-mΩ, T0-220 package) and three 30CTQ100 Schottky diode pairs (100-V, 2 × 30 A, T0-220 package), locally bypassed with three 0.47-μF ceramic capacitors. Note that the voltage ratings of the semiconductor devices were selected quite conservatively, as testing demonstrated that voltage transients could be limited below 56 V, even under load-dump conditions (see Section III). The MOSFETs are driven from IR4426S gate drivers via 4.7-Ω series resistors. Control is provided by a MC68HC908 microcontroller, which controls both the SMR and provides pulsewidth modulated (PWM) field control. The SMR operates at a switching frequency of 100 kHz, representing a reasonable tradeoff between switching and conduction loss, while the field is pulsewidth modulated at 12.5 kHz.

A custom aluminum heat sink was designed based on thermal models for the alternator developed in [17] and [23]; a photograph of the devices mounted to the heat sink is shown in Fig. 4. Acceptable temperature rises at the device cases of less than 50 °C were found for all operating conditions evaluated.

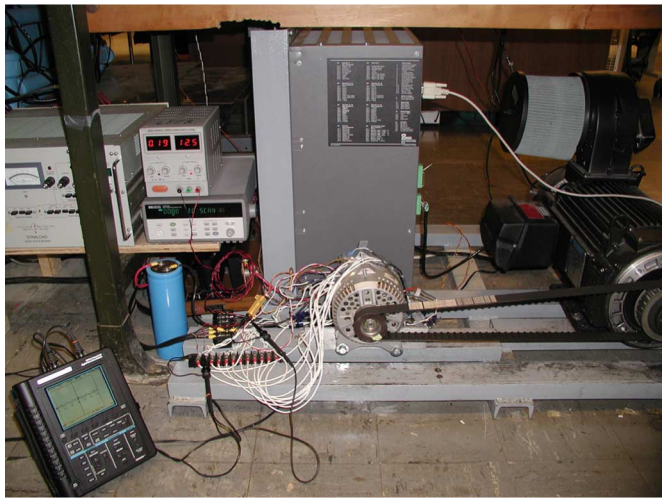

Fig. 8. The experimental setup used to test the prototype system. The system enables measurement of voltages, currents, and temperatures across a wide range of drive and load conditions. Details of the experimental apparatus and methods may be found in [26].

An interesting result in this thermal design was the temperature difference between the FETs and their heat sink, and the diodes and their heat sink (detailed in [26]). With only one exception, the heat sink was always hotter than the silicon device. The FETs and diodes are exposed to the coolest air, as the fan draws air past the semiconductors, through the heat sink, and then blows it over the alternator windings. Apparently, the heat generated in the semiconductors is completely carried away by the air flowing over them. Because the heat sink is thermally connected to the case and the windings, it also helps to carry away some of the heat from the windings. To reduce the temperature of the semiconductors, it would probably be better to thermally isolate them from the case of the alternator and the windings. This is a slightly different thermal design from what was built for this experiment. Further details of the electrical and thermal design and testing of the SMR may be found in [23]–[26].

III. Control

Control of the alternator encompasses a number of tasks. Foremost is the regulation of the output voltage across variations in load. This is achieved through control of both the alternator field current and the switching pattern of the rectifier. Control of the field and SMR should also be performed in a manner that meets other goals, such as maintaining high efficiency and controlling output ripple. Additionally, there is a need to handle fault conditions. One requirement is to limit the "load-dump" voltage transient that can occur when the battery is suddenly disconnected from the alternator while drawing high current [34]–[43]. In this section, we describe how these control requirements are addressed in the prototype system, and present experimental results that validate our methods. A photograph of the experimental setup is shown in Fig. 8.

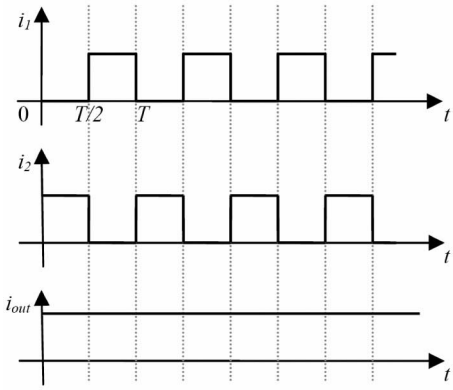

Fig. 9. Example of ripple cancellation with interleaving for two interleaved cells.

A. SMR Control

Multiple possibilities exist for controlling the output voltage and current of the interleaved alternator configuration of Fig. 3. In each case, one selects a combination of field current and duty ratio that provides sufficient power to regulate the output. One straightforward possibility is to operate the interleaved system exactly as a single-cell design, but with the gating waveforms of the cells interleaved appropriately. For example, one might select the field current and duty ratio according to the efficiency-optimizing controller of [10], and simply phase shift the gating waveforms to the individual cells by appropriate amounts. With this strategy, the switching ripple current into the output capacitor is reduced by an amount that depends on the number of cells and the duty ratio, and the fundamental switching ripple frequency is increased by a factor N_C (e.g., see [25] and [28]–[33]).

Another control possibility arises from the fact that the switching ripple currents delivered by the interleaved cells cancel completely for certain duty ratios (e.g., see [25] and [28]–[30]), yielding an output waveform that is ideally free of switching ripple. For example, as illustrated in Fig. 9, in a two-cell system operating at a 50% duty ratio ($d = 0.5$), the pulsating currents from the individual cells add to provide a continuous (small-ripple) output current waveform. Thus, a two-cell system can ideally be operated at $d = 0$ (corresponding to diode rectification) or $d = 0.5$ with minimal switching ripple. Likewise, in a four-cell system ($N_C = 4$), the cell switching ripple currents cancel completely for duty ratios d of 0, 0.25, 0.5, and 0.75, respectively. By accepting operation at only these specific duty cycles, significant reductions in capacitor rating and filtering requirements can be achieved at the expense of design complexity.

The alternator design demonstrated here takes advantage of this "perfect cancellation" interleaving strategy. Because we constrain the control to only discrete duty ratios, the load-matching condition indicated in (2) and illustrated in Fig. 2 is not achieved precisely across speed. However, in our four-cell design, there is sufficient flexibility with four available duty ratios ($d = 0$, 0.25, 0.5, and 0.75, respectively) to make a reasonable approximation to load-matched performance at heavy

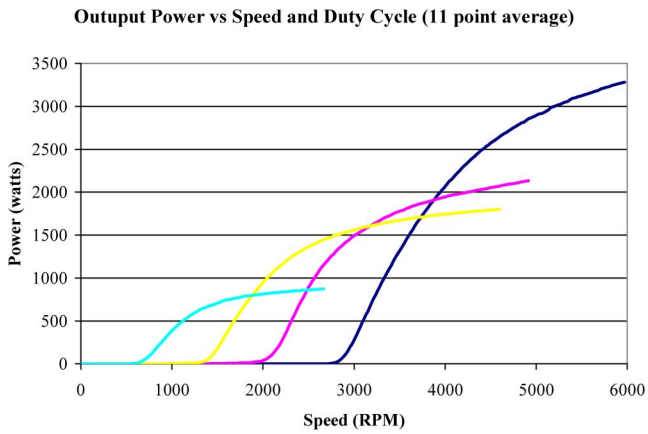

Fig. 10. Experimental output power at full field and each allowed duty ratio (rising from left to right: $d = 0.75$, 0.5, 0.25, and 0, respectively).

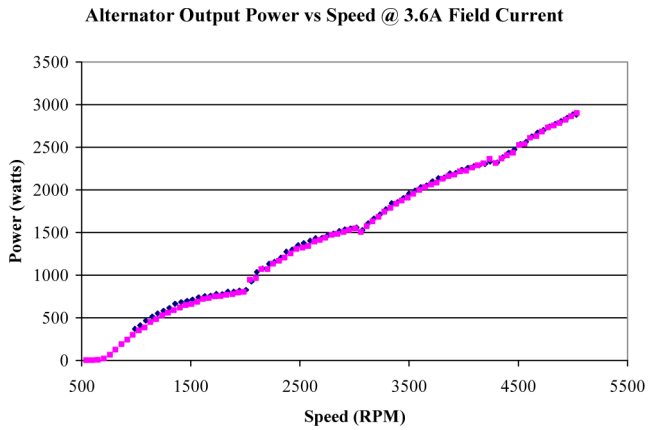

Fig. 11. Experimental output power at full field with automatic duty-ratio switching. Dark dots are for rising speed, light dots are for falling speed.

TABLE I
TRANSITION SPEEDS FOR INCREASING AND DECREASING THE SMR DUTY RATIO

Transition Table		
Duty Cycles	Transition Speed for Decreasing d	Transition Speed for Increasing d
0.5, 0.75	2001 rpm	1744 rpm
0.25, 0.5	3212 rpm	2839 rpm
0, 0.25	4360 rpm	3938 rpm

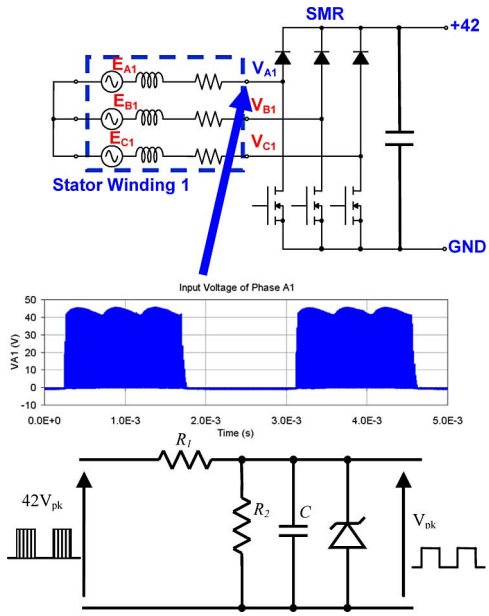

Fig. 12. Circuit and method for detecting alternator speed and phase current direction. This information is used in controlling the SMR duty ratio and implementing synchronous rectification.

loads. Fig. 10 shows experimental measurements of alternator output power at full field current and at each of these duty ratios across speed. Fig. 11 demonstrates automatic duty-ratio switching to achieve near load-matched power across speed; the two curves illustrate performance for increasing and decreasing speed, respectively.

B. Output Voltage Regulation

Given the selected restriction to a discrete set of SMR duty ratios for ripple cancellation, the question arises of how to maintain output regulation across alternator speed and load. The strategy adopted in our prototype system is to select an appropriate duty ratio based on alternator speed (with a small amount of hysteresis in the transition points), and to regulate the output power within that speed range via field control. Table I shows the transition speeds for switching among the allowed duty ratios, and illustrates the hysteresis in the transitions.

In realizing this control scheme, there is a need to detect the alternator speed. Fig. 12 illustrates the method and circuitry for detecting alternator speed. The pulsating voltage at the drains of three SMR MOSFETs are measured and filtered to provide a set of digital signals. Each signal indicates the direction of the current of that alternator phase. By measuring the period of the signals, the electrical frequency and alternator speed is easily determined. Moreover, these signals can be used for implementing partial synchronous rectification (as described in the following).

Alternator field current is adjusted between 0 and a maximum value (nominally 3.6 A) by PWM. As the field is wound for a 14-V output, but is driven from 42 V in our design, the field duty ratio is limited to a maximum value of 28% (below 33%). Field duty ratio is adjusted based on output voltage error mainly via proportional control, with a voltage deviation of ± 2.68 V causing a field duty-ratio swing between zero and maximum. A small summed error term (digital integral term) is also added into the field duty ratio to provide good steady-state performance, but the gain of this integral term is sufficiently small that it does not compromise the dynamics of the proportional control.

Fig. 13 shows how field current varies as a function of speed to maintain the desired output at a variety of loads ranging from 100 to 2500 W. The speed points where the duty-ratio transitions occur are clearly visible. Fig. 14 shows output power versus speed for the alternator for a number of fixed load currents. Notice how the effect of duty- transitions and field current variations and transitions cancel to produce the desired constant

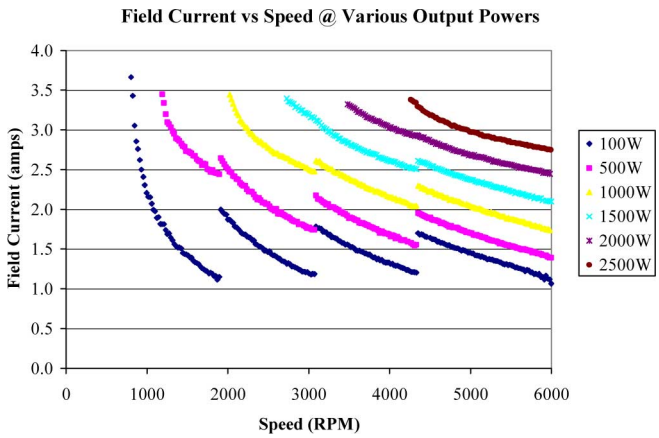

Fig. 13. Experimental measurement of field current (scale 0–4 A) versus alternator speed at various output power levels (100, 500, 1000, 1500, 2000, and 2500 W, respectively).

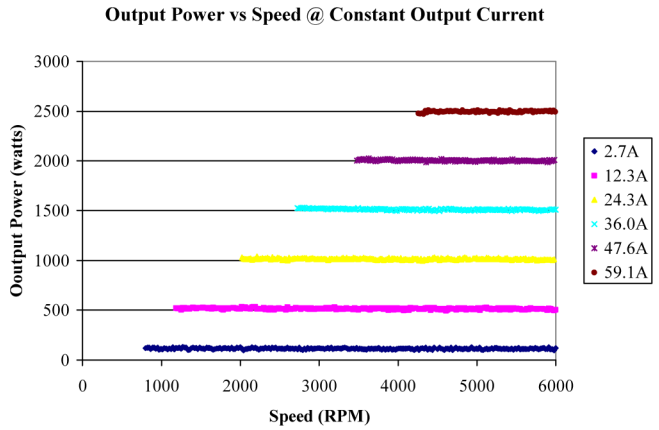

Fig. 14. Experimental measurement of output power (scale 0–3000 W) versus alternator speed at various load current levels (2.7, 12.3, 24.3, 36.0, 47.6, and 59.1 A, respectively).

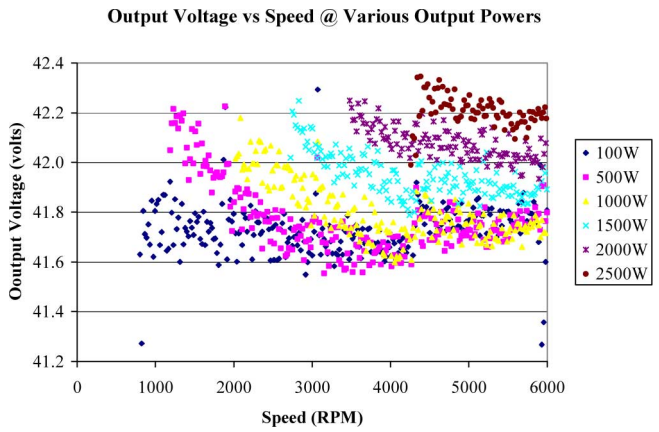

Fig. 15. Experimental measurement of output voltage (scale 41.2–42.4 V) across speed (scale 0–6000 r/min) at output power levels from 100 to 2500 W.

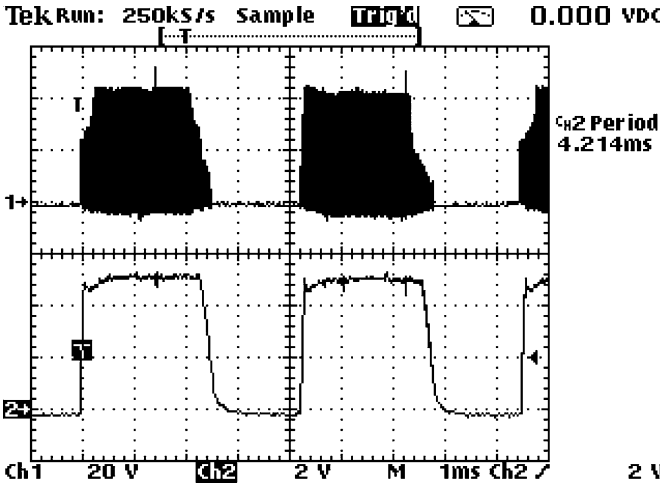

Fig. 16. Experimental measurement of a MOSFET drain voltage (Ch1) and the digital phase current direction signal (Ch2) generated by the circuit of Fig. 12.

power across speed. Fig. 15 shows a scatter plot of the alternator output voltage across speed and load power; almost all of the points fall within ± 0.4 V of the set point of 42 V. These results demonstrate the ability to regulate the output across a wide range of speed and load with the proposed control approach.

C. Synchronous Rectification

In order to maintain high efficiency, it is desirable to achieve at least partial synchronous rectification with the MOSFETs in the SMR . That is, in order to reduce loss, we would like to turn the MOSFETs ON when the phase currents would otherwise pass through the MOSFET body diodes. This requires some means to detect the direction of the phase current. We achieve this without the need for direct current measurements using the approach illustrated in Fig. 12 and described earlier. Fig. 16 illustrates the pulsating drain voltage of the MOSFET along with the digital signal to the microprocessor indicating phase current direction. The digital signals indicating phase current direction are used to synthesize synchronous rectification pulses to hold the MOSFETs ON during the appropriate time period. Note that when the MOSFET is held ON, we cannot detect a direction change for the phase current with this method. Because of this, and to accommodate the fact that the span of the desired ON pulse varies with speed and load, we only set the synchronous rectification pulsewidth to 85% of the time indicated by our detection scheme, thus providing some operating margin. Moreover, whenever the alternator first starts up or changes duty ratio, the synchronous rectification pulses are turned off and then slowly increased to their 85% duration over a number of cycles. This allows efficient operation under steady-state conditions without causing problems during transients.

Testing of the proposed synchronous rectification scheme demonstrated its efficacy. It was found that synchronous rectification always provides an improvement in operating temperatures of the SMR . Considering the worst case thermal points for the SMR at each duty ratio, it was found that synchronous rectification lowered diode temperature an average of 4.6 °C and MOSFET temperature an average of 7.4 °C (on the order of 10% of total temperature rise). Detailed measurements for a

variety of operating conditions may be found in [26]. As there is no additional hardware expense and little control complexity to realizing the proposed synchronous rectification scheme, its use is well justified.

D. Load-Dump Transient Control

Control of load-dump transients is another important aspect of alternator design. This is particularly important in 42-V electrical systems, since the proposed transient limits [27] are much tighter (on a percent overvoltage basis) than is typically achieved with Lundell alternators (e.g., see [34]–[43]). The SMR alternator can achieve significantly improved output voltage transient response as compared to a diode-rectified alternator [10]. When a load dump event takes place, the output current of the alternator has no place to go; therefore, the output voltage builds up. If the increase in output voltage is sensed, and the MOSFETs in the rectifier are turned on when the voltage exceeds a threshold, the alternator current can be diverted from the output while the field current is reduced, and the high-voltage transient associated with the energy stored in the machine synchronous reactance can be eliminated. Moreover, shorting the output of the machine via the MOSFETs prevents the line-to-line back EMF voltage of the alternator from appearing at the rectifier output. The strategy undertaken is thus to detect the occurrence of a load-dump transient overvoltage with a comparator. When a fault is detected, the SMR MOSFETs are turned on, and the field drive is turned off. After a minimum 300 ms delay for clearance of the fault, the alternator restarts.

To demonstrate this load-dump control strategy, the output of the alternator was connected to a switched resistor network, without the presence of a battery or large capacitive filter. Only a small 60-μF capacitance was included at the alternator output in addition to the 6.1-μF of bypass capacitors on the SMR printed circuit board. The switched resistor network was configured to permit the load resistance to be rapidly switched from 0.58 to 42 Ω (72 A to 1 A/3024 W to 42 W).

Fig. 17 shows the example results for alternator operation at 4500 r/min (0% duty cycle) and an initial load 72 A. As the load dump is detected, alternator output current is cut off (diverted through the SMR MOSFETs). The transient voltage rises to a peak of approximately 58 V at a rate of about 1.3 V/μs. Repeated testing demonstrated the ability to limit peak overvoltage at the alternator output to 58 V. Note that during the load-dump suppression, the rectifier MOSFETs see higher than the usual current. Measurements of the MOSFET currents show that they peak at about 56 A, and decay approximately with the same time constant as the field current. As the MOSFETs in this design have a peak current rating of 140 A and the overcurrent lasts only a very short time (50–100 ms), there is no danger of damage to the alternator or the external system.

It may be concluded that tight load-dump control is achieved in the prototype system. Control of the SMR under full-scale load-dump transients yields a peak overvoltage of only 58 V on the 42-V system, without undue stress on the semiconductor devices.

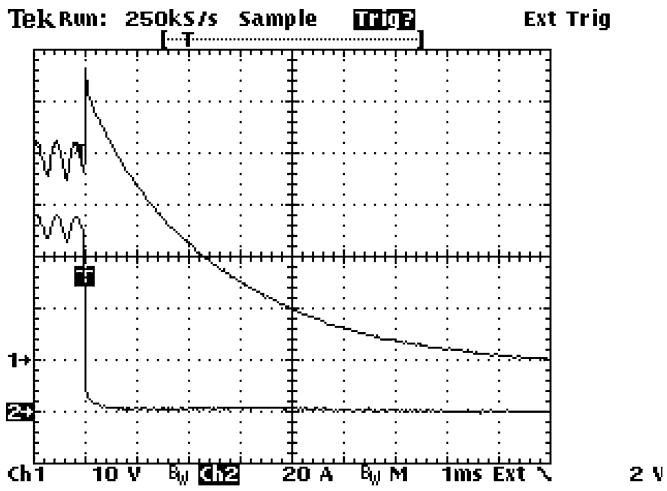

Fig. 17. Load-dump transient response for a load step from 0.58 to 42 Ω (from $\sim$3024 to $\sim$42 W) at 4500 r/min with no battery. Channel 1 shows alternator output voltage, while channel 2 shows alternator output current. The output voltage transient is limited to 58 V.

IV. Conclusion

This paper presents techniques for the design of high-power Lundell alternators with integrated SMR s. A multisection stator winding and interleaved rectifier arrangement is introduced that enables high power levels to be achieved using small semiconductor devices, and which greatly reduces the output filter capacitor requirements. We also demonstrate control methods suited to this interleaved system. In addition to accurate closed-loop output voltage control, we introduce methods to provide (partial) synchronous rectification for reduced loss, and to provide tight load-dump transient control. The proposed technology is validated in the design and experimental evaluation of a 42-V, 3.4-kW alternator with fully integrated power electronics and controls. The prototype alternator achieves approximately a factor of 2.1 increase in power and 1.6 increase in power density as compared to a conventional diode-rectified alternator, along with a substantial improvement in load-dump performance.

References

[1] G. Henneberger, "Improvement of the output performance of the claw-pole alternators by additional permanent magnets," presented at the Int. Conf. Electric Mach., Paris, France, 1994.

[2] M. Naidu, M. Boules, and R. Henry, "A High Efficiency, High Power Generation System for Automobiles," in *Proc. IEEE Ind. Appl. Soc. Annu. Meeting*, 1995, pp. 709–716.

[3] F. Liang, J. Miller, and S. Zarei, "A control scheme to maximize output power of a synchronous alternator in a vehicle electrical power generation system," in *Proc. IEEE Ind. Appl. Soc. Annu. Meeting*, Oct. 1996, pp. 830–835.

[4] F. Liang, J. Miller, and X. Xu, "A vehicle electrical power generation system with improved output power and efficiency," *IEEE Trans. Ind. Appl.*, vol. 35, no. 6, pp. 1341–1346, Nov./Dec. 1999.

[5] H. Ishikawa, A. Umeda, and M. Kohmura, "Development of a more efficient and higher power generation technology for future electrical systems," presented at the Int. Congr. Transp. Electron. (Convergence 2000), Detroit, MI, Oct., SAE Paper 2000-01-C081.

[6] A. L. Julian and G. Oriti, "New brushless alternator for automotive applications," in *Proc. IEEE Ind. Appl. Soc. Annu. Meeting*, Sep./Oct. 2001, pp. 443–448.

[7] I. Boldea, S. Scridon, and L. Tutelea, "BEGA- A biaxial excitation generator for automobiles," presented at the 7th Int. OPTIM Conf., Brasov, Romania, May 10–11, 2000.
[8] F. B. Reiter Jr., K. Rajashekara, and R. J. Krefta, "Salient pole generators for belt-driven automotive alternator applications," in *Proc. IEEE Ind. Appl. Soc. Annu. Meeting*, 2001, pp. 437–442.
[9] S. Scridon, I. Boldea, L. Tutelea, F. Blaabjerg, and A. E. Richie, "BEGA – A biaxial excitation generator for automobiles: Comprehensive characterization and test results," *IEEE Trans. Ind. Appl.*, vol. 41, no. 4, pp. 935–944, Jul./Aug. 2005.
[10] D. J. Perreault and V. Caliskan, "Automotive power generation and control," *IEEE Trans. Power Electron.*, vol. 19, no. 3, pp. 618–630, May 2004.
[11] J. M. Rivas, D. J. Perreault, and T. A. Keim, "Performance improvement in alternators with switched-mode rectifiers," *IEEE Trans. Energy Convers.*, vol. 19, no. 3, pp. 561–568, Sep. 2004.
[12] W. L. Soong and N. Ertugrul, "Inverterless high-power interior permanent-magnet automotive alternator," *IEEE Trans. Ind. Appl.*, vol. 40, no. 4, pp. 1083–1091, Jul./Aug. 2004.
[13] C.-Z. Liaw, D. M. Whaley, W. L. Soong, and N. Ertugrul, "Investigation of inverterless control of interior permanent-magnet alternators," *IEEE Trans. Ind. Appl.*, vol. 42, no. 2, pp. 536–544, Mar./Apr. 2006.
[14] C. Z. Liaw, W. L. Soong, and N. Ertugrul, "Closed-loop control and performance of an inverterless interior PM automotive alternator," in *Proc. Conf. Power Electron. Drive Syst.*, 2005, pp. 343–348.
[15] C. Z. Liaw, W. L. Soong, and N. Ertugrul, "Low-speed output power improvement of an interior PM automotive alternator," in *Proc. IEEE Ind. Appl. Soc. Annu. Meeting*, 2006, pp. 27–34.
[16] G. Hassan, D. J. Perreault, and T. A. Keim, "Design of dual-output alternators with switched-mode rectification," *IEEE Trans. Power Electron.*, vol. 20, no. 1, pp. 164–172, Jan. 2005.
[17] S. C. Tang, T. A. Keim, and D. J. Perreault, "Thermal modeling of lundell alternators," *IEEE Trans. Energy Convers.*, vol. 20, no. 1, pp. 25–36, Mar. 2005.
[18] L. M. Lorilla, T. A. Keim, J. H. Lang, and D. J. Perreault, "Topologies for future automotive generators, Part I: Modeling and analytics," presented at the Veh. Power Propulsion Conf., Chicago, IL, Sep. 2005.
[19] L. M. Lorilla, T. A. Keim, J. H. Lang, and D. J. Perreault, "Topologies for future automotive generators, Part II: Optimization," presented at the Veh. Power Propulsion Conf., Chicago, IL, Sep. 2005.
[20] D. J. Perreault, T. A. Keim, J. H. Lang, and L. M. Lorilla, "Applications of power electronics in automotive power generation," presented at the SIA Int. Conf. Automotive Power Electron., Paris, France, Jun. 2006.
[21] L. M. Lorilla, T. A. Keim, J. H. Lang, and D. J. Perreault, "Foil field lundell alternator with rotating power electronics," in *Proc. IEEE Power Electron. Spec. Conf.*, Jeju, Korea, Jun. 2006, pp. 2164–2169.
[22] S. Rees and U. Ammann, "A smart synchronous rectifier for 12 V automobile alternators," in *Proc. IEEE Power Electron. Spec. Conf.*, 2003, pp. 1516–1521.
[23] S. C. Tang, D. J. Perreault, and T. A. Keim, "Advanced automotive power electronics: Thermal analysis of lundell alternator," MIT/Ind. Consortium Adv. Automotive Electr./Electron. Compon. Syst., Summer 2002 Project Rep., Sep. 2002.
[24] S. C. Tang, D. J. Perreault, and T. A. Keim, "Advanced automotive power electronics: Switching behavior of power MOSFETs in switched-mode-rectifier for lundell alternator," MIT/Ind. Consortium Adv. Automotive Electr./Electron. Compon. Syst., Winter 2003 Project Rep., Jan. 14, 2003.
[25] S. C. Tang, D. J. Perreault, and T. A. Keim, "Electronically-aided power generation and control: Design principle of interleaved switched mode rectifier for lundell alternator," MIT/Ind. Consortium Adv. Automotive Electr./Electron. Compon. Syst., Summer 2003 Project Rep., Aug. 21, 2003.
[26] D. Otten, "Test report: Switch mode rectifier equipped alternator," *MIT Laboratory for Electromagnetic and Electronic Systems*, Sep. 2006.
[27] J. M. Miller, D. Goel, D. Kaminski, H.-P. Schöner, and T. M. Jahns, "Making the case for a next generation automotive electrical system," in *Proc. IEEE-SAE Int. Conf. Transp. Electron. (Convergence)*, Dearborn, MI, Oct.1998, pp. 41–51, SAE Paper 98C006.
[28] C. Chang and M. Knights, "Interleaving technique in distributed power conversion systems," *IEEE Trans. Circuits Syst. I, Fundam. Theory Appl.*, vol. 42, no. 5, pp. 245–251, May 1995.
[29] D. J. Perreault and J. G. Kassakian, "Distributed interleaving of paralleled power converters," *IEEE Trans. Circuits Syst. I, Fundam. Theory Appl.*, vol. 44, no. 8, pp. 728–734, Aug. 1997.
[30] B. A. Miwa, D. M. Otten, and M. F. Schlecht, "High efficiency power factor correction using interleaving techniques," in *Proc. IEEE Appl. Power Electron. Conf.*, Boston, MA, 1992, pp. 557–568.
[31] B. A. Miwa, "Interleaved conversion techniques for high density power supplies," Ph.D. dissertation, Dept. Electr. Eng. Comput. Sci., MIT, Cambridge, MA, Jun. 1992.
[32] B. N. Singh, G. Joos, and P. Jain, "A new topology of 3-phase PWM AC/DC interleaved converter for telecommunication supply systems," in *Proc. IEEE Ind. Appl. Soc. Annu. Meeting*, Oct. 2000, pp. 2290–2296.
[33] D. J. Perreault and J. G. Kassakian, "Design and evaluation of a cellular rectifier system with distributed control," *IEEE Trans. Ind. Electron.*, vol. 46, no. 3, pp. 495–503, Jun. 1999.
[34] D. J. Perreault, K. K. Afridi, and I. A. Khan, "Automotive applications of power electronics," in *The Power Electronics Handbook*, M. H. Rashid, Ed. New York: Academic, 2001, pp. 791–813.
[35] SAE EMI Standards Committee (1995), "Immunity to conducted transients on power leads," SAE Standard J1113/11, in *SAE Handbook*, Society of Automotive Engineers, Warrendale, PA, 1999.
[36] J. R. Morgan, "Transients in the automotive electrical system," in *Proc. Veh. Technol. Conf.*, Cleveland, OH, 1973, pp. 1–10.
[37] S. Yamamoto, O. Ozeki, T. Yamanaka, and H. Kondo, "Electrical environmental characteristics for automotive electronic systems," *IEEE Trans. Veh. Technol.*, vol. VT-32, no. 2, pp. 151–157, May 1983.
[38] S. Korn, "Automobiles need transient voltage suppression," *Power Convers. Intell. Motion*, vol. 15, no. 2, pp. 28–31, Feb. 1989.
[39] T. Elfland, M. Manternach, A. Marshall, and J. Mings, "The load dump," in *Proc. IEEE Workshop Electron. Appl. Transp.*, 1990, pp. 73–78.
[40] J. D. Dimech, "Standardized automotive load dump testing," in *Proc. IEEE Int. Symp. Electromagn. Compat.*, 1991, pp. 355–359.
[41] P. Le Bars, "42 V load dump transient and centralised active suppression," in *Proc. Passenger Car Electr. Arch. IEE Semin.*, London, U.K., 2000, pp. 4/1–4/3.
[42] C. S. Namuduri, B. V. Murty, and M. G. Reynolds, "Load dump transient control of a 42V automotive generator," in *Proc. IEEE Power Electron. Spec. Conf.*, Aachen, Germany, 2004, pp. 389–394.
[43] Z. J. Shen, S. P. Robb, F. Y. Rob, M. Fuchs, D. Berels, and K. Hampton, "Load dump protection in 42 V automotive electrical distribution systems," in *Proc. IEEE Appl. Power Electron. Conf.*, 2001, pp. 289–295.
[44] S. C. Tang, D. M. Otten, T. A. Keim, and D. J. Perreault, "Design and evaluation of a 42 V automotive alternator with integrated switched-mode rectifier," in *Proc. IEEE Veh. Power Propulsion Conf.*, Sep. 2007, pp. 250–258.

Sai Chun Tang (S'97–M'01) was born in Hong Kong in 1972. He received the B.Eng. degree (with first class honors), and the Ph.D. degree in electronic engineering from City University of Hong Kong, Kowloon, Hong Kong, in 1997 and 2000, respectively.

He was a Research Fellow at the City University of Hong Kong. He joined the National University of Ireland, Galway, Ireland as a Visiting Academic Research Fellow in 2001, and then the Laboratory for Electromagnetic and Electronic Systems, Massachusetts Institute of Technology, Cambridge, in 2002. Since 2004, he has been at the Focused Ultrasound Laboratory, Brigham and Women's Hospital, Harvard Medical School, Boston, MA, where he has been involved in the development of ultrasound diagnosis devices and noninvasive treatment systems using high-intensity focused ultrasound. In 2008, he became a Faculty Member at Harvard Medical School and an Instructor in radiology. His research interests include high-frequency electromagnetism, low-profile power converter design, and analog electronics.

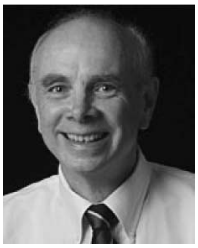

David M. Otten received the B.S. and S.M. degrees from the Massachusetts Institute of Technology (MIT), Cambridge, in 1973 and 1974, respectively.

In 1974, he joined the Electric Power Systems Engineering Laboratory, MIT as a Staff Engineer. Since 1984, he has been a Principal Research Engineer in the Laboratory for Electromagnetic and Electronic System, MIT. His current research interests include instrumentation, power electronics, and the micromouse robot contest.

Thomas A. Keim received the D.Sc. degree from the Massachusetts Institute of Technology (MIT), Cambridge.

He was at MIT for several years as a Member of the sponsored research staff, where he was involved in superconducting electric machines. He was for over a decade with General Electric Corporate Research and Development (now known as GE Global Research), where he was involved in superconducting electric machines and in superconducting electromagnets for medical nuclear magnetic resonance imaging. He was a Corporate Officer and Chief Engineer at Kaman Electromagnetics Corporation (now a part of DRS Technologies, Inc.) for nearly a decade and led engineering of multiple high-performance electromechanical and power electronics systems. Since 1998, he has again been at MIT, where he is a Principal Research Engineer and the Director of the MIT/Industry Consortium on Advanced Automotive Electrical/Electronic Components and Systems. He has authored or coauthored more than 45 publications in various international journals and conferences, and holds 11 patents.

David J. Perreault (S'91–M'97–SM'06) received the B.S. degree from Boston University, Boston, MA, in 1989, and the S.M. and Ph.D. degrees from the Massachusetts Institute of Technology (MIT), Cambridge, MA, in 1991 and 1997, respectively.

In 1997, he joined the Laboratory for Electromagnetic and Electronic Systems, MIT as a Postdoctoral Associate, and became a Research Scientist in 1999. In 2001, he joined the Department of Electrical Engineering and Computer Science, MIT, where he is currently an Associate Professor. He has coauthored four IEEE prize papers. His research interests include design, manufacturing, and control techniques for power electronics, and their use in a wide range of applications.

Dr. Perreault received the Richard M. Bass Outstanding Young Power Electronics Engineer Award from the IEEE Power Electronics Society, an Office of Naval Research Young Investigator Award, and the Society of Automotive Engineers Ralph R. Teetor Educational Award.